energies

MDPI

Article

Validation and Application of CFD Methodology for Core Inlet Flow Distribution in APR1000 Reactor

Sung Man Son, Won Man Park, Dae Kyung Choi and Choengryul Choi *

ELSOLTEC, 1401-2, 184 Jungbu-daero, Giheung-gu, Yougin-si 17095, Gyeonggi-do, Republic of Korea; ssm@elsoltec.com (S.M.S.); wmpark@elsoltec.com (W.M.P.); cdk@elsoltec.com (D.K.C.)
* Correspondence: crchoi@elsoltec.com

Abstract: The core inlet flow distribution in the APR1000 reactor is critical for ensuring the reactors safety and efficient operation by maintaining uniform coolant flow across fuel assemblies. Previous studies, though insightful, faced challenges in fully replicating reactor-scale flow conditions due to technical and economic constraints associated with scaled-down experimental models and the limited numerical validation methodologies. This study addresses these limitations by developing and validating a robust computational fluid dynamics (CFD) methodology to accurately analyze the core inlet flow distribution. A 1/5 scaled-down experimental model adhering to similarity laws was employed for validation. CFD analyses using ANSYS Fluent and CFX, combined with turbulence model evaluations and grid sensitivity studies, demonstrated that the SST and RNG k-ε turbulence models provided the most accurate predictions, with a high correlation to previous experimental data. Full-scale simulations revealed uniform coolant distribution at the core inlet, with peripheral assemblies exhibiting higher flow rates, consistent with previous experimental observations. Quantitative metrics such as the coefficient of variation (COV), relative error (RD), and root mean square error (RMSE) confirmed the superior performance of the SST model in CFX, achieving a COV of 7.993% (experimental COV: 5.694%) and an RD of 0.047. This methodology not only validates the CFD approach but also highlights its applicability to reactor design optimization and safety assessment. The findings of this study provide critical guidelines for analyzing complex thermal-fluid systems in nuclear reactor designs.

Keywords: APR1000 reactor; 1/5 scale-down model; core inlet flow distribution; computational fluid dynamics (CFD); grid sensitivity; turbulence model sensitivity

Academic Editors: Rosa Lo Frano and Rodrigue Largenton

Received: 4 December 2024
Revised: 11 January 2025
Accepted: 15 January 2025
Published: 23 January 2025

Citation: Son, S.M.; Park, W.M.; Choi, D.K.; Choi, C. Validation and Application of CFD Methodology for Core Inlet Flow Distribution in APR1000 Reactor. *Energies* **2025**, *18*, 512. https://doi.org/10.3390/en18030512

1. Introduction

The APR1000 (Advanced Power Reactor 1000) is a next-generation pressurized light water reactor that is being developed to reflect the latest technologies and requirements based on the OPR1000, a Korean standard nuclear power plant [1,2]. The stability and efficient operation of the APR1000 reactor are primarily determined by its cooling performance, which effectively removes the heat generated from nuclear fuel. The cooling performance is a critical factor in ensuring reactor safety by reliably removing thermal power from the reactor and controlling the temperature of nuclear fuel [3–5]. A decline in cooling performance can lead to severe safety incidents such as core damage and core melt. Notably, the majority of the heat generated in the reactor originates from the nuclear fuel within the core. Therefore, the flow distribution within the core and the heat transfer efficiency of the coolant are major concerns in the thermal-hydraulic design and analysis of the reactor.

A key variable influencing the cooling performance is the core inlet flow distribution, which determines whether the coolant is uniformly distributed to each fuel assembly (FA) and channel [3–5]. If the uniformity of the coolant flow is not maintained, excessive heat accumulation (local hotspots) may occur in specific channels, significantly increasing the risk of thermo-mechanical damage. Thus, accurately analyzing the core flow distribution and optimizing it during the design phase are essential processes in the stable operation of the reactor. However, precisely measuring complex thermal-fluid interactions under actual operating conditions is challenging due to experimental, technical, and economic constraints.

To overcome these limitations, an approach combining experimental research and numerical analysis is employed. Kim et al. [1,2] designed and fabricated a scaled-down model to experimentally obtain the core inlet flow distribution of the APR1000 reactor. This scaled-down model reflects the thermal-hydraulic characteristics under the high-temperature and high-pressure operating conditions of the reactor. To ensure geometric and hydrodynamic similarity, the design concept of the ACOP (Advanced Core Flow & Pressure) experimental facility was applied [6]. The primary objective of this experimental setup was to accurately capture the core inlet flow distribution, aintaining geometric similarity to the reactor core. The linear dimensions of the reactor were scaled down by a factor of 1/5 to allow for geometric similarity, and 177 core simulators were installed to replicate the fuel assembly arrangement of the APR1000 reactor. Additionally, to achieve hydrodynamic similarity, the coolant velocity was reduced to half compared to the full-scale reactor, and experiments were conducted accordingly [1,6,7].

While scaled-down model experiments provide valuable data and insights, achieving perfect similarity with actual reactor conditions is difficult, and there are limitations in terms of time and cost. As a complementary approach to these experimental methods, computational fluid dynamics (CFD) analysis has emerged as a flexible and powerful alternative capable of analyzing thermal-fluid behavior under various operating conditions.

CFD analysis technology is being applied across various fields, including mechanical, architectural, food, medical, and oil industries [8–18]. Since its introduction to the nuclear field in the mid-1990s, CFD analysis has been widely utilized in reactor design, operational optimization, and safety analysis [19–23]. CFD analysis offers the high-resolution analysis of flow fields and heat transfer, and can simulate complex geometries and diverse operating conditions. However, CFD results can be highly sensitive to factors such as the grid resolution, turbulence models, numerical schemes, and software used. Therefore, establishing appropriate analytical methods and validating them against actual data are essential for reliable CFD analysis.

In this study, we aim to develop a robust CFD analysis methodology for evaluating the coolant flow distribution at the core inlet of the APR1000 reactor and to validate this approach effectively. To achieve this objective, CFD analyses were conducted on both scaled-down and full-scale models of the reactor. The validation of the analytical methods was performed by comparing the CFD results from the scaled-down model with available experimental data, addressing the lack of experimental data for the full-scale APR1000 model. This validation process ensured the reliability of the CFD methodology, which was subsequently applied to analyze the core inlet flow distribution of the full-scale APR1000 model. To guarantee the accuracy and reproducibility of the CFD results, comprehensive analyses were undertaken, including grid sensitivity studies, turbulence model evaluations, and cross-comparisons using different commercial CFD software packages. These steps are critical in establishing confidence in the simulation outcomes. The validated CFD methodology provides essential fundamental data that supports the stable operation and design optimization of the APR1000 reactor. Furthermore, the findings offer valuable

insights for optimizing reactor design and enhancing safety assessments by confirming the high reliability of analysis of the full-scale model analysis through comparisons with scaled-down experimental results. Additionally, the CFD analysis methodology developed in this study is versatile and can be extended to other reactor designs and complex thermal-fluid systems, serving as a pivotal guideline for future design and analysis efforts.

This manuscript is organized as follows. First, the development of the analysis models is detailed, and both the scaled-down and full-scale APR1000 reactor models are introduced. Second, the analysis methods are described, covering the numerical techniques, mesh generation, and boundary condition settings used for the CFD simulations. Third, the results from the scaled-down model analysis are presented and compared with experimental data to validate the analytical methods. Finally, the analysis results of the full-scale model are discussed, providing an in-depth examination of the core inlet flow distribution in the APR1000 reactor.

2. APR1000 Reactor

The APR1000 reactor is designed as a pressurized water reactor (PWR), which reliably remove heat generated from nuclear fission reactions through heat exchange with the coolant. The reactor is equipped with a total of 177 fuel assemblies arranged in a 15×15 configuration (HIPER16). Each fuel assembly consists of fuel rods, spacer grids, upper and lower nozzles, and guide tubes. The fuel assemblies transfer the heat generated from the fission reactions to the coolant, which absorbs the heat and continuously removes it by circulating along the flow paths.

To maintain the uniformity and stability of the coolant flow, the APR1000 reactor is designed to optimize the interactions between major components. The coolant enters the reactor through four cold legs (CLs), forming a descending flow along the downcomer (DC) (Figures 1 and 2). The downcomer stabilizes the descending flow of the coolant and delivers it to the lower plenum, ensuring uniform distribution to the fuel assemblies. The uniform distribution in the lower plenum guarantees that each fuel assembly is evenly cooled, preventing local overheating within the assemblies. The fuel assemblies located in the core transfer the heat generated from fission reactions to the coolant, which is heated as it absorbs the heat. The heated coolant then moves to the upper plenum and is discharged outside the reactor through the hot legs (HLs). Subsequently, the coolant releases heat in the steam generator (SG) and is cooled before being supplied back to the cold legs via the reactor coolant pumps (RCPs), ensuring continuous and stable heat removal from the reactor.

To further ensure the uniformity and stability of the coolant flow, the APR1000 reactor incorporates a core bypass flow path. The core bypass flow path directs a portion of the coolant to bypass the fuel assemblies, ensuring balanced coolant flow distribution and preventing local heat accumulation in specific channels. Structures such as alignment keys, a core shroud annulus, and outlet nozzle gaps are designed to naturally distribute the coolant flow, maintaining the overall flow stability and enhancing the flow balance within the entire system.

The APR1000 reactor includes multiple safety systems to ensure stable heat removal even under emergency conditions. Among these, the emergency core barrel duct (ECBD) plays a crucial role by directly supplying coolant to the fuel assemblies during emergencies, assisting in heat removal. The ECBD provides an additional critical pathway for core cooling, thereby maintaining the cooling performance and enhancing reactor safety.

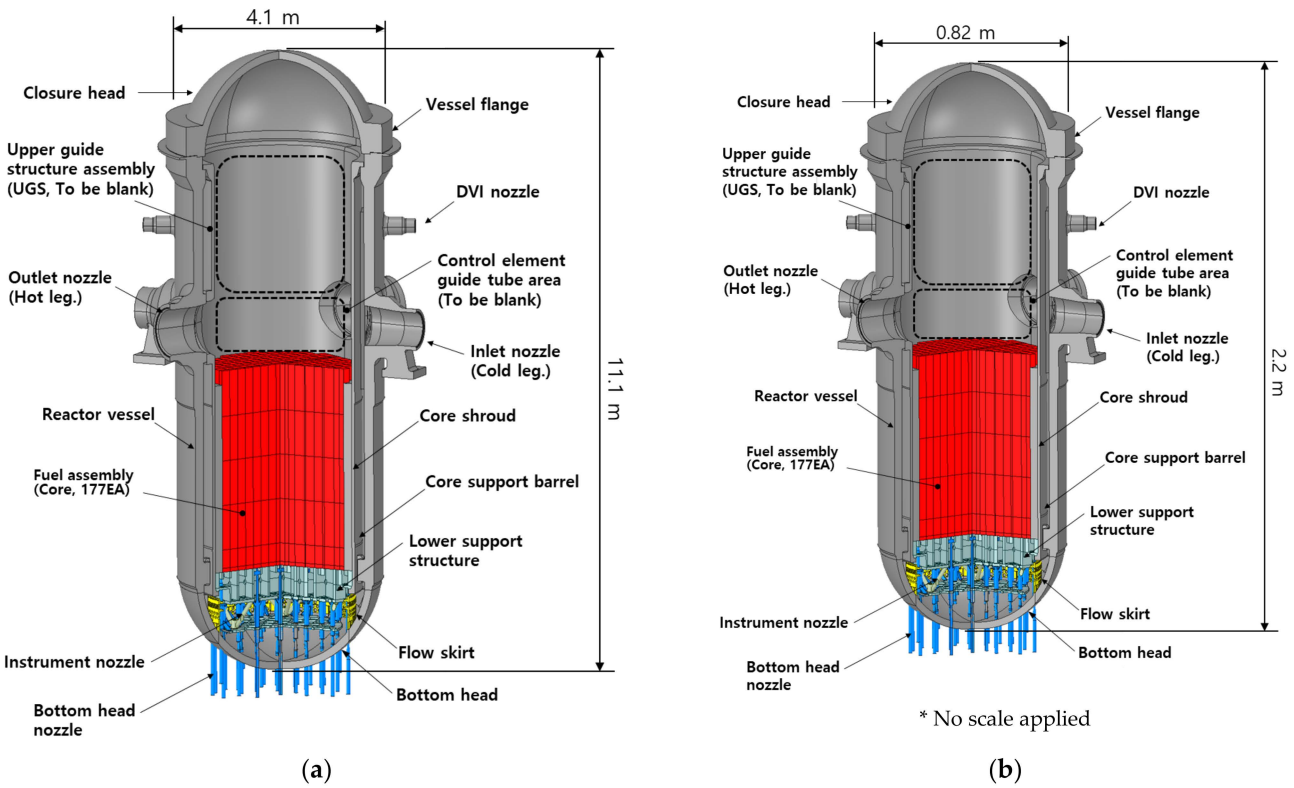

Figure 1. CFD analysis model for APR1000 reactor: (**a**) full scale model; (**b**) 1/5 scaled-down model.

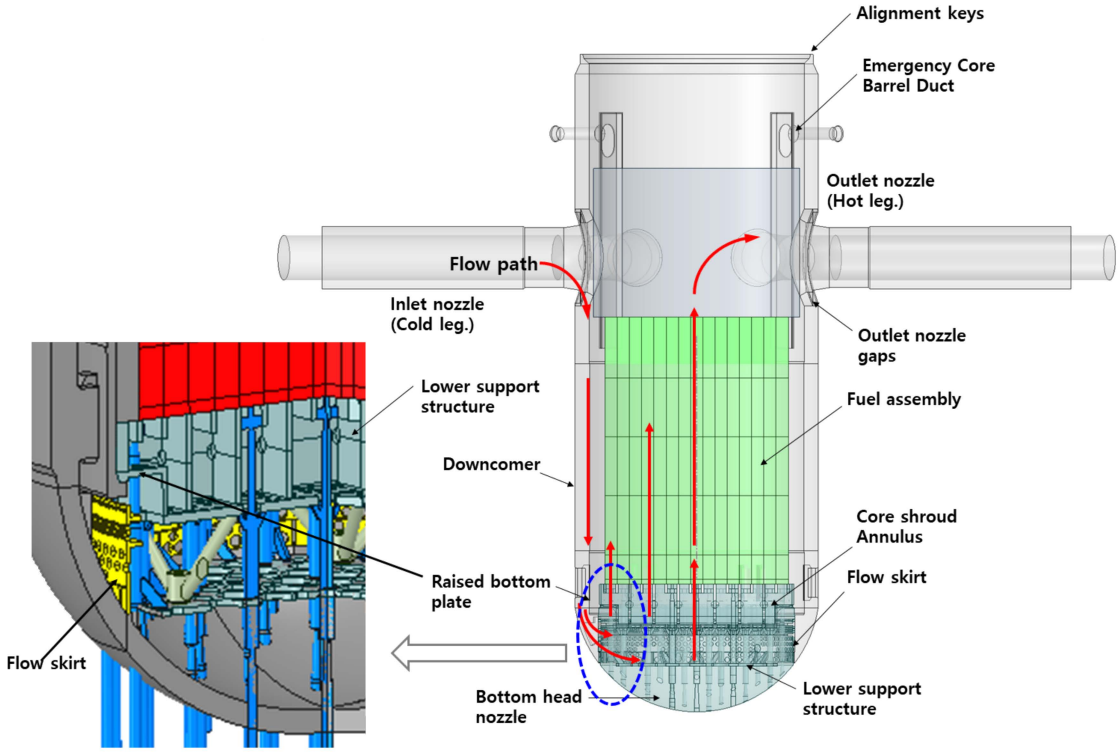

Figure 2. Schematic of coolant flow path of APR1000.

3. CFD Analysis Methodology

3.1. CFD Analysis Model and Grid System

Based on the design data of the APR1000 reactor, a three-dimensional full-scale geometric model was created for CFD analysis (Figure 1a). Since this study focuses on analyzing the core inlet flow distribution of the APR1000 reactor, the flow path from the cold leg to the core inlet was constructed by nearly 100% reflecting the geometric information of the structures. In contrast, the flow path from the core inlet to the upper plenum, including the hot leg, was not an exact replicate of the geometric details of the structures. Regions such as the area containing the 177 fuel assemblies, the tube bank region, and the upper guide structure (UGS) region within the core were modeled using a porous media model during the CFD analysis to simulate axial and lateral pressure drops without detailed geometric considerations. If these regions were modeled with full geometric detail, the complexity would significantly increase the required number of grids, resulting in excessive computation time. The scaled-down model was fabricated as a 1/5 scale model, consistent with Kim et al. [1,2], and was linearly scaled down (Figure 1b).

The grid system for the full-scale APR1000 reactor CFD analysis was developed using the fabricated three-dimensional full-scale geometric model. To maintain grid consistency, the grid system for the scaled-down model was created by scaling down the full-scale grid system (Figure 3). During the grid generation, a combination of tetrahedral and hexahedral grids was used to account for the complexity of the geometry. Finer grids were applied in regions with expected significant variations in their physical quantities to enhance the accuracy of the analysis. As previously mentioned, CFD analysis results can be influenced by the grid used; therefore, to evaluate the grid sensitivity, three grid systems (coarse: y+ = 370, intermediate: y+ = 300, fine: y+ = 100) were created based on the average y+ obtained through preliminary analysis. The grid densities of each grid system are summarized in Table 1.

3.2. CFD Analysis Conditions

The conditions applied to the full-scale and scaled-down models of the APR1000 reactor during CFD analysis are presented in Tables 2 and 3, respectively. Each model was established under different thermal-hydraulic conditions to simulate the actual operating thermal-fluid behavior of the full-scale model and to validate the CFD analysis methodology using experimental data from the scaled-down model.

Table 1. Grid density for each region in 1/5 scaled-down model.

Region	Grid Density (no. of Cells/m^3)		
	Coarse (y+ = 370)	**Intermediate (y+ = 300)**	**Fine (y+ = 100)**
Cold Legs	61,692,753	61,828,440	78,628,282
Downcomer	66,950,601	86,399,952	183,455,470
Lower Plenum	110,066,770	129,389,836	263,751,298
Fuel Assembly	9,489,224	10,470,021	15,891,037
Upper Plenum	10,937,712	10,957,224	11,085,108
Hot Legs	11,753,197	12,627,618	19,415,999
Average	40,619,301	47,839,252	90,520,452

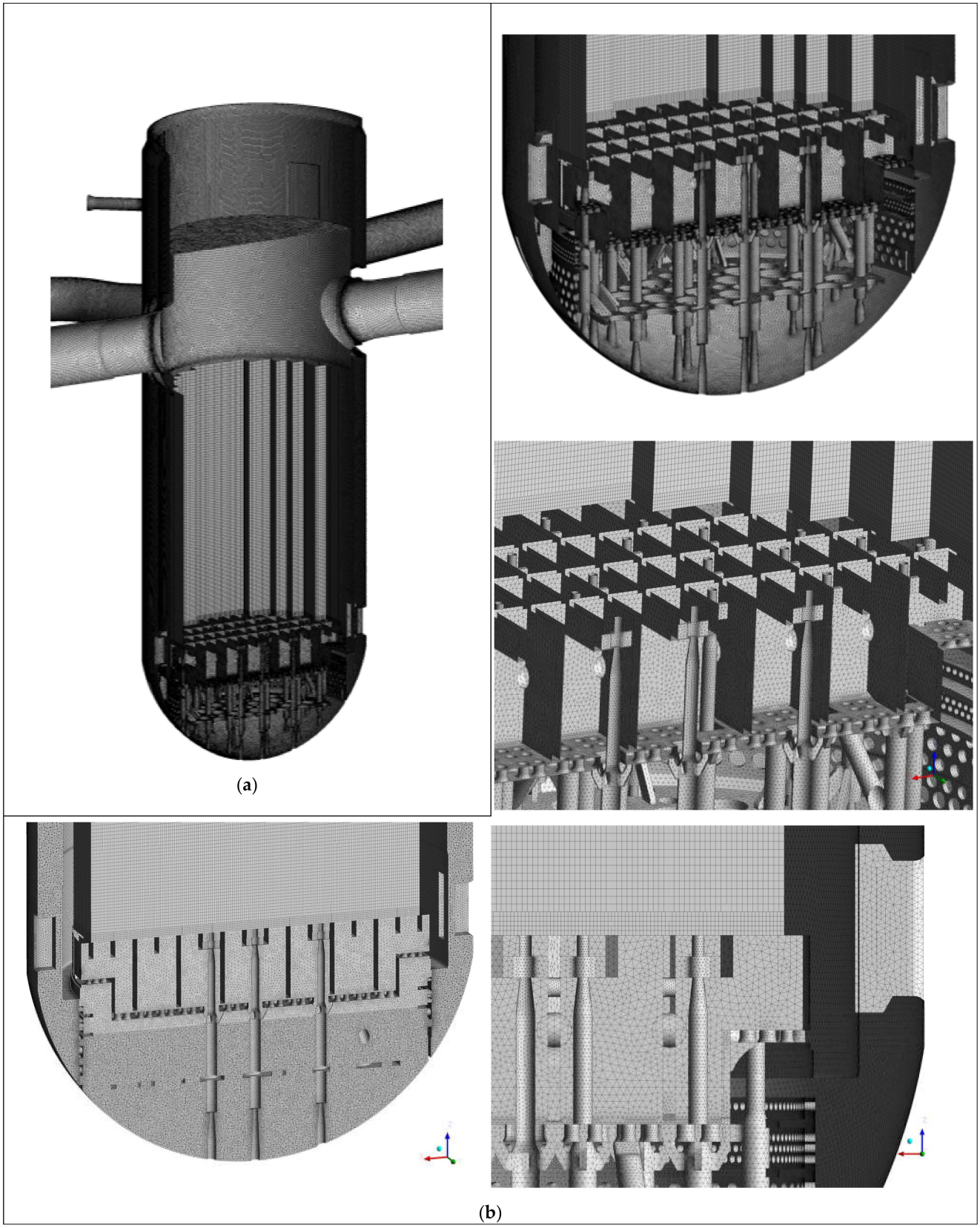

Figure 3. Grid system for APR1000 reactor (1/5 scaled-down model, coarse grid system): (**a**) overall; (**b**) lower plenum.

Table 2. CFD analysis conditions for original and 1/5 scale models.

Location		Full-Scale Model				1/5 Scaled-Down Model (Experiment [2])			
		Flow Rate		Temp.	Pressure	Flow Rate		Temp.	Pressure
		(kg/s)	(kg/s)	(°C)	(MPa)	(kg/s)	(kg/s)	(°C)	(MPa)
Cold Leg	CL1A	3827	15,308	295.8	-	100	400	60.0	-
	CL2A	3827				100			
	CL2B	3827				100			
	CL1B	3827				100			
Hot Leg	HL1	7654	15,308	-	15.5	200	400	-	0.2
	HL2	7654				200			
Core Bypass	Alignment Keys	N/A	2% *	-	-	-	-	-	-
	Outlet Nozzle Gaps	N/A		-	-	-	-	-	-
	Core Shroud Annulus	N/A		-	-	-	-	-	-

* Flow ratio compared to the total flow entering the reactor.

Table 3. Inertia resistance factors for porous media regions.

Region	Direction	Full-Scale Model	1/5 Scaled-Down Model
		(m^{-1})	(m^{-1})
Core (FA)	Axial	4.540	22.837
	Lateral	108.960	548.088
Upper Plenum (Tube Bank and UGS)	Axial	3.990	27.957
	Lateral	3.990	27.957

For the full-scale model, the analysis conditions were based on the actual reactor design operating conditions. The coolant enters through four cold legs (velocity inlet), each with a flow rate of 3827 kg/s, resulting in a total inflow rate of 15,308 kg/s. The outflow was set through two hot legs (pressure outlet), each with a flow rate of 7654 kg/s, balancing the inflow and outflow rates. The coolant inlet temperature was set at 295.8 °C, and the outlet pressure at 15.5 MPa, reflecting the reactor's high-temperature and high-pressure conditions. Additionally, the core bypass flow path was defined to include pathways such as alignment keys, outlet nozzle gaps, and a core shroud annulus, with approximately 2% of the total flow bypassing the core.

In CFD analysis, the core region is modeled as a porous medium by introducing a momentum source term in the momentum equations. This momentum source term accounts for the resistance to fluid flow within the porous medium and consists of two components: the viscous loss term and the inertia loss term. The viscous loss term represents resistance due to fluid viscosity, while the inertia loss term accounts for resistance caused by changes in fluid velocity. These terms are expressed as follows:

$$S = -\left(\frac{\mu}{K_{p,i}} v_i + K_i \frac{1}{2} \rho |v| v_i\right)$$

In this equation:

- S: momentum source term, representing the resistance force per unit volume acting on the fluid due to the porous medium.
- μ: dynamic viscosity of the fluid (Pa·s), which represents the fluid's resistance to shear deformation;
- K_p: permeability of the porous medium (m^2), which quantifies how easily fluid can flow through the medium;
- v_i: component of the velocity vector in the i-th direction (m/s);
- K_i: inertia resistance factor (1/m), which represents the contribution of inertia effects to flow resistance;
- ρ: density of the fluid (kg/m^3);
- $|v|$: magnitude of the velocity vector (m/s).

This approach is utilized to accurately model the resistance characteristics of fluid flow within porous media. In this study, only the inertia loss term was considered for the CFD analysis.

In the porous media region of the full-scale model, the axial inertia resistance coefficient was set to 4.540 m^{-1}, and the lateral inertia resistance coefficient to 108.960 m^{-1}. For the upper plenum, both the axial and lateral inertia resistance coefficients were uniformly set to 3.990 m^{-1}. These values were determined using design data and through preliminary analysis. It was assumed that there was no heat release from the fuel assemblies within the core region.

The scaled-down model applied simplified thermal-hydraulic conditions identical to those used in Kim et al.'s experiment [2]. In the scaled-down model, coolant enters through four cold legs, each with a flow rate of 100 kg/s, resulting in a total inflow rate of 400 kg/s.

The outflow was set through two hot legs, each with a flow rate of 200 kg/s, maintaining a balance between the inflow and outflow rates. The coolant inlet temperature was set at 60.0 °C, and the outlet pressure at 0.2 MPa, reflecting low-temperature and low-pressure conditions imposed by experimental constraints. Similarly to the experiments, no core bypass flow was included in the scaled-down model. In the porous media region, the axial inertia resistance coefficient was set to 22.837 m^{-1}, and the lateral inertia resistance coefficient to 548.088 m^{-1}. For the upper plenum, both the axial and lateral inertia resistance coefficients were set to 27.957 m^{-1}. These values were determined based on the design data of the scaled-down experimental facility and preliminary analysis. As with the full-scale model, it was assumed that there was no heat release from the fuel assemblies within the core region.

3.3. Numerical Method

In this study, CFD analysis was performed to analyze the core inlet flow distribution characteristics within the APR1000 reactor. The fundamental equations used were the continuity equation, momentum equation, and energy equation. To accurately represent complex turbulence characteristics, the selection of an appropriate turbulence model is essential. Based on existing studies [24–28], four representative turbulence models—the standard k-ε (or k-ε in CFX), SST (shear stress transport), RNG k-ε, and RSM (Reynolds stress model, LRR Reynolds Stress in CFX)—were applied to perform CFD analyses on both the full-scale and scaled-down models. Each turbulence model was selected considering the characteristics and computational efficiency under various flow and thermal-fluid conditions. The standard k-ε model is widely used due to its computational efficiency and simplicity. The SST model was developed to enhance the accuracy near walls and overall flow field predictions. The RNG k-ε model is an improved model that is capable of precisely simulating the detailed distribution of turbulent energy. The RSM directly

calculates the Reynolds stress, allowing for a more accurate representation of turbulence characteristics in complex flows.

To ensure the reliability and consistency of the CFD analysis results, analyses were conducted using two commercial CFD software packages, ANSYS Fluent and ANSYS CFX, under identical analysis conditions. In Fluent, the SIMPLE algorithm was used for pressure–velocity coupling, and a second-order upwind scheme was applied as the discretization method to enhance the spatial accuracy in the flow analysis. Conversely, using CFX, we employed a pressure-based coupled solver, simultaneously solving pressure and velocity equations to achieve fast and stable convergence. A high-resolution scheme was used for discretization, and the time scale factor was set to 1.0 to ensure computational stability. For both CFD software packages, the convergence criteria were set such that all residuals were below 10^{-3}, ensuring the accuracy and stability of the analysis.

4. Results and Discussion

4.1. 1/5 Scaled-Down Model

Figure 4 presents the CFD analysis results obtained for the scaled-down APR1000 reactor model using the k-ε turbulence model in CFX with a coarse mesh system. To visually represent the coolant flow characteristics within the APR1000 reactor, the results are divided into the (a) overall coolant flow and (b) coolant flow in the lower plenum. The overall coolant flow illustrates the entire flow path, showing coolant entering through the cold legs, passing through the downcomer (DC) and lower plenum, flowing through the fuel assemblies, and finally exiting through the hot legs. It is evident that the coolant is uniformly distributed within the reactor and flows along the designed paths. Specifically, it is clear that the coolant entering the lower plenum is uniformly distributed before flowing to the fuel assemblies.

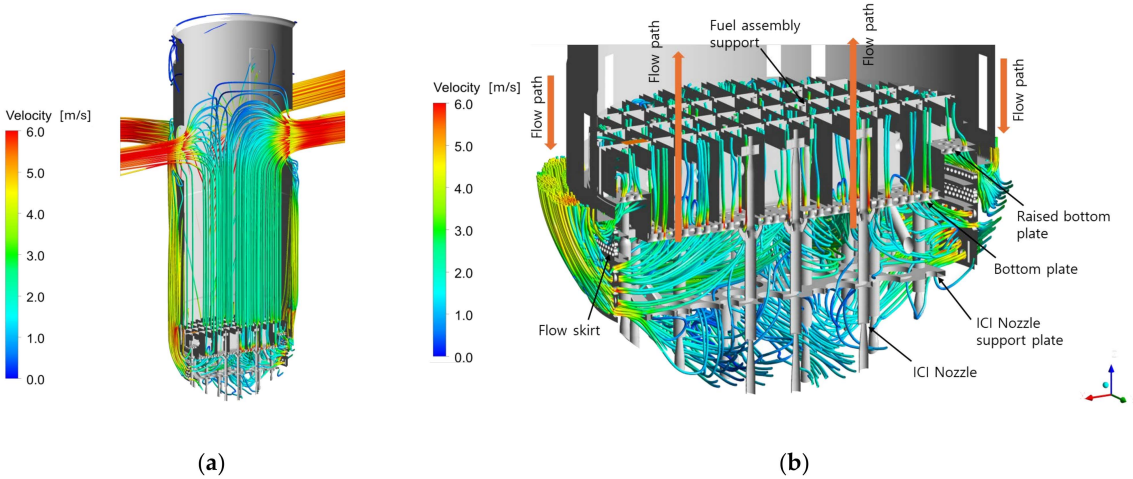

(**a**) (**b**)

Figure 4. Coolant flow in the reactor: overall flow and lower plenum distribution in the 1/5 scale-down model. (**a**) Overall coolant flow; (**b**) coolant flow in lower plenum.

The coolant flow in the lower plenum provides a detailed view of the flow distribution before the coolant is delivered to the fuel assemblies. After entering through the cold legs, the coolant is distributed along structures such as the flow skirt, bottom plate, and raised bottom plate within the lower plenum. These structures are designed to induce flow uniformity, and the changes in the flow velocity along the flow paths are visually observable. The velocity distribution within the lower plenum ranged from 1.0 to 5.0 m/s, indicating the formation of a uniform flow distribution. Additionally, localized increases in the flow velocity were observed as the coolant passed through structures like the ICI

nozzle support plate. These results demonstrate the effective operation of the structures designed to ensure uniform coolant distribution within the reactor. Particularly, the process of uniformly dispersing the flow as it passes through the complex structures of the lower plenum plays a crucial role in optimizing the cooling efficiency.

To evaluate the grid sensitivity in the scaled-down model of the APR1000 reactor, CFD analyses were performed using three grid resolutions—coarse, intermediate, and fine—within Fluent. Figure 5 visually depicts the flow distribution at the core inlet, showing an increasing trend of coolant flow toward the core periphery under each grid condition. While there are local differences in flow distribution across all grid conditions, the overall distribution remains uniform, effectively reflecting the key features of the core design and flow distribution. These results confirm the effectiveness of the structures designed to ensure the even distribution of coolant throughout the core.

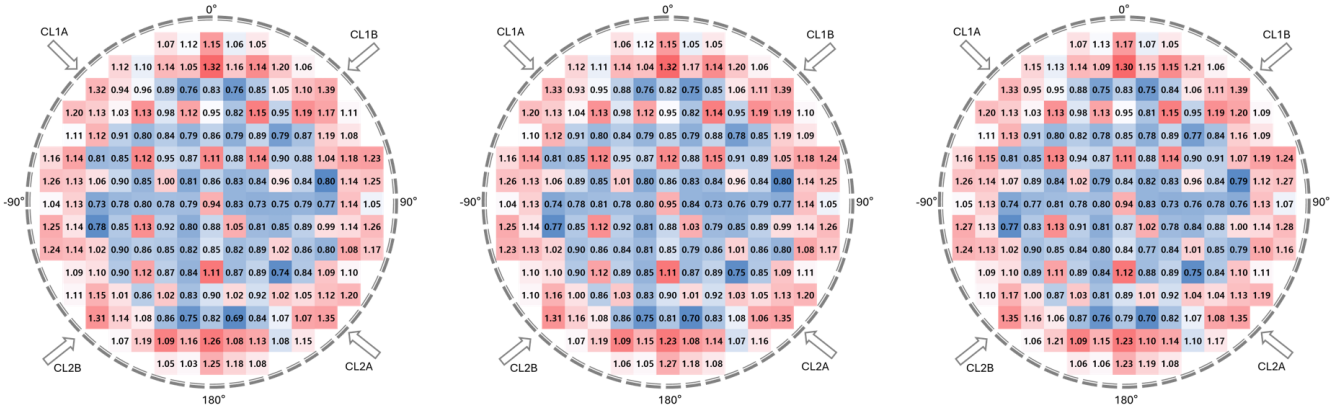

Figure 5. Core inlet flow distribution across different grid resolutions. (**a**) Coarse; (**b**) intermediate; (**c**) fine.

Figure 6 graphically represents the dimensionless flow distribution at the eighth row and eighth column to provide a more detailed view of the flow distribution data presented in Figure 5. This graph clearly shows the changes in flow distribution along specific paths, confirming that the overall trend of flow distribution remains consistent across all grid conditions. These results indicate that the grid resolution does not significantly impact the main characteristics of the flow distribution, providing sufficient evidence that the method used herein accurately captures the overall flow trends.

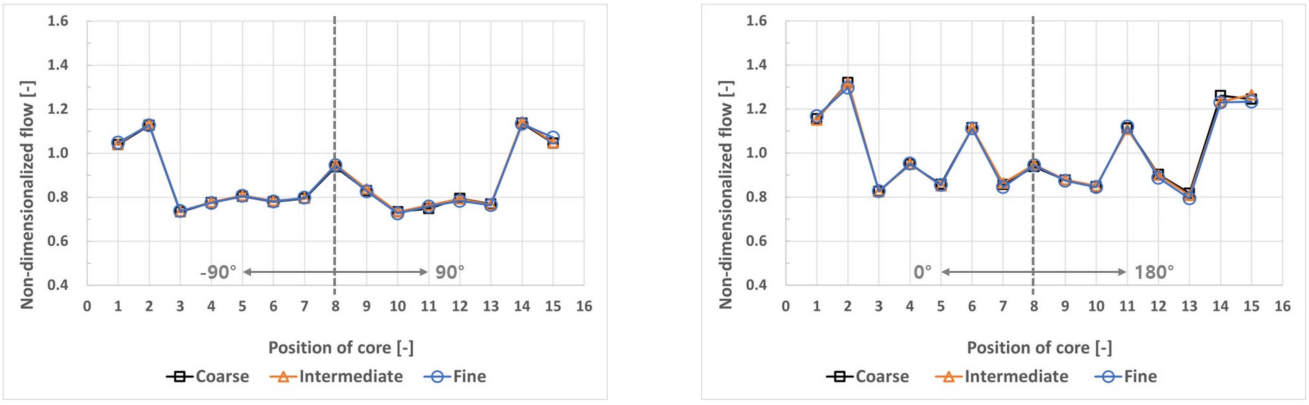

Figure 6. Comparison of core inlet flow distribution along the eighth row and column across different grid systems. (**a**) Eighth row; (**b**) eighth column.

Table 4 summarizes the statistical characteristics of the flow distribution for each grid resolution. The minimum and maximum flow rates remain consistently within the range from 0.685 (0.703) to 1.385 (1.386), indicating a minimal impact of the grid resolution on extreme values. The coefficient of variation (COV) was 15.80% for the coarse grid and 16.28% for the fine grid, showing a slight increase with a higher grid resolution; however, this difference does not significantly affect the overall flow trend. Overall, the primary trends in the flow distribution are similar across all grid resolutions, confirming that the coarse grid is a practically effective choice when considering computational efficiency. This demonstrates that using a coarse grid for core inlet flow analysis in the APR1000 reactor is effective for design reviews and large-scale analyses, balancing computational cost and accuracy.

Table 4. Grid sensitivity of core inlet flow distribution.

	Coarse	**Intermediate**	**Fine**
Min. Flow Rate (-)	0.685	0.700	0.703
Max. Flow Rate (-)	1.385	1.390	1.385
Coefficient of variation (COV) (%)	15.8	15.9	16.3

To evaluate the turbulence model sensitivity in the scaled-down model of the APR1000 reactor, CFD analyses were performed using four turbulence models: standard k-ε, SST, RNG k-ε, and the RSM. By analyzing the differences in the core inlet flow distribution resulting from the use of different turbulence models, the sensitivity of the turbulence models was assessed. These analyses were conducted using both Fluent and CFX software to compare results between the two platforms. Finally, the analysis results were validated by comparing them with experimental data. A coarse grid was used in this process to consider computational efficiency.

Figures 7 and 8 illustrate the core inlet flow distribution as visualized by Fluent and CFX, respectively, for each turbulence model. These figures show detailed differences in flow distribution depending on the turbulence model used. Overall, all turbulence models exhibited an increasing trend in flow towards the core periphery, similar to the experimental results (Figure 9). Specifically, the SST and RNG k-ε models accurately reproduced flow distributions that were similar to the experimental data compared to the other turbulence models.

Figures 10 and 11 present the dimensionless flow distributions at the eighth row and eighth column, quantitatively comparing the flow variations due to the use of different turbulence models. Both software packages maintain consistent overall trends across turbulence models, with local differences present but the general flow distribution shape remaining similar. Figure 12 shows the experimental data-based flow distribution at the same row and column positions, revealing differences in the central region but an overall matching trend with the analysis results.

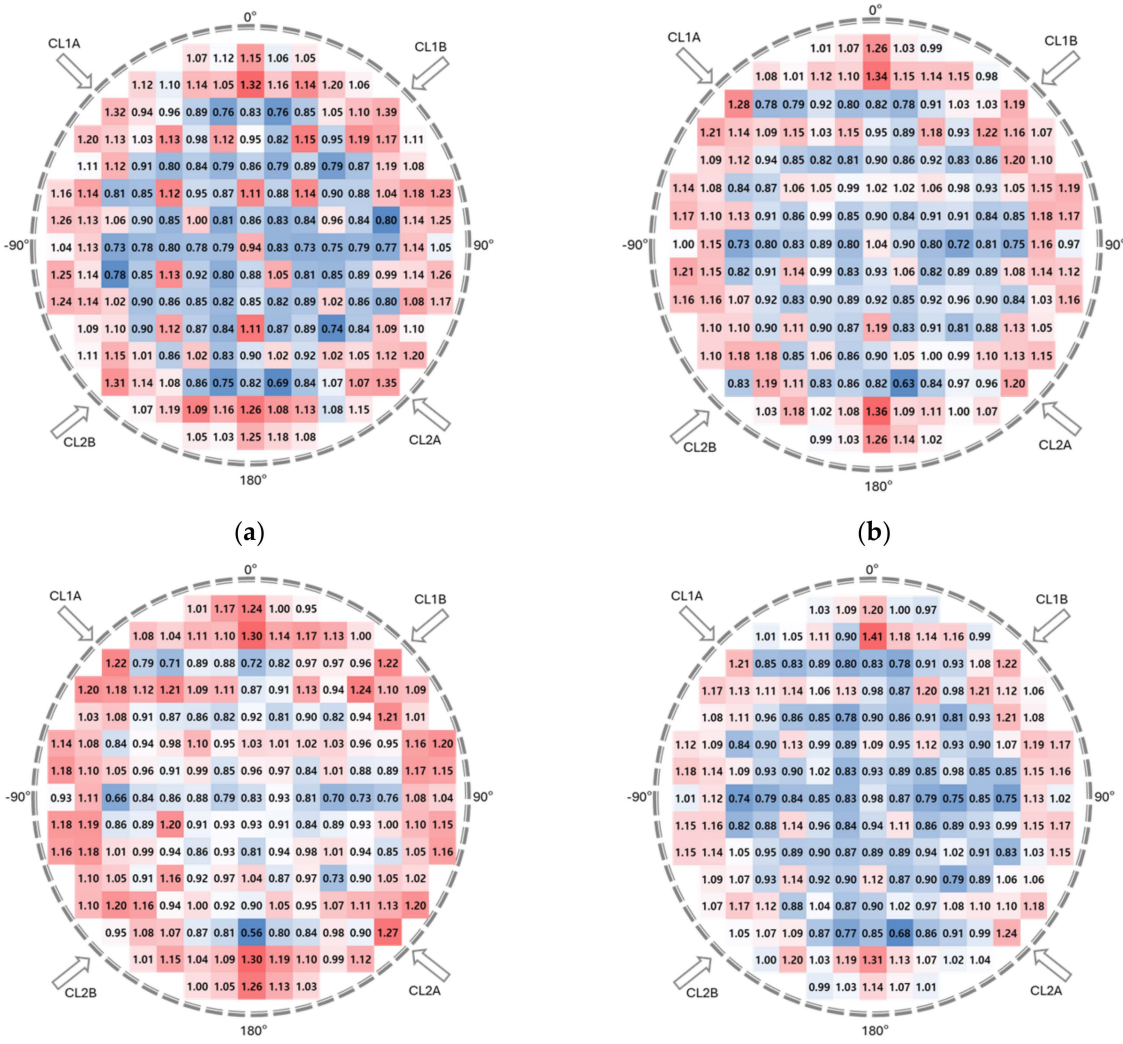

Figure 7. Core inlet flow distribution according to turbulence models (FLUENT) in the 1/5 scale-down model: (**a**) standard k-ε; (**b**) SST; (**c**) RNG k-ε; (**d**) RSM.

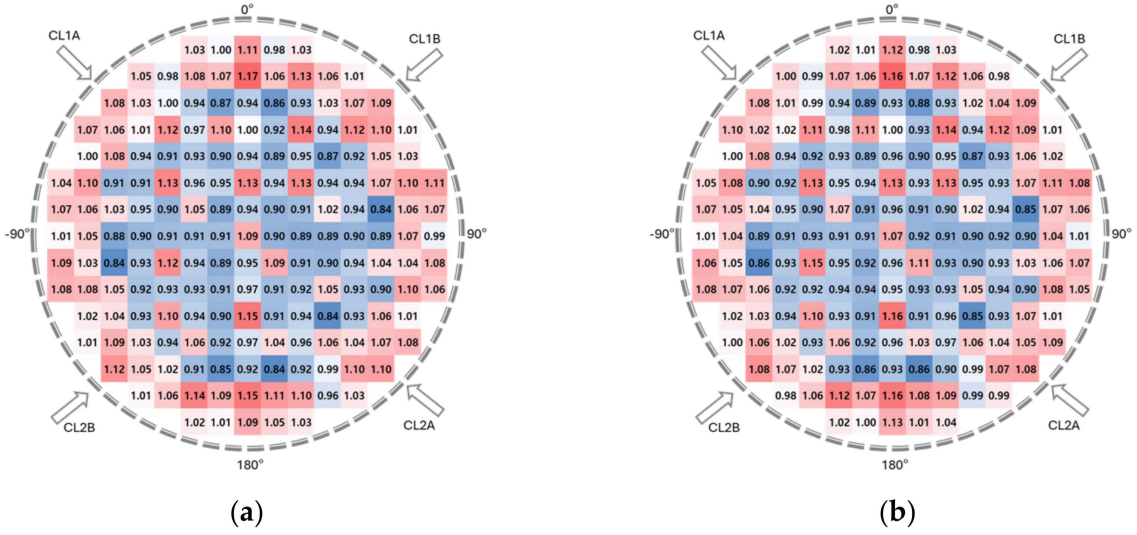

Figure 8. *Cont.*

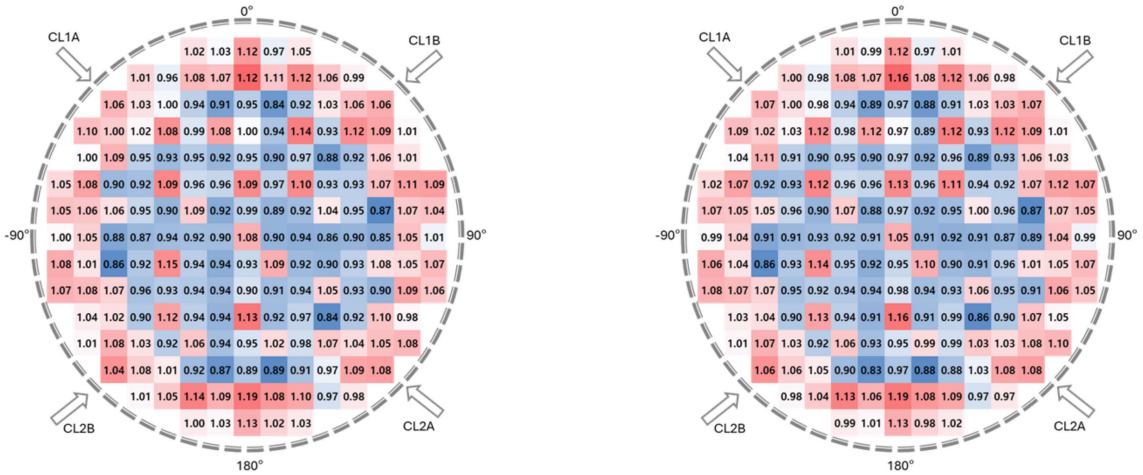

(**c**) (**d**)

Figure 8. Core inlet flow distribution according to turbulence models (CFX) in the 1/5 scale-down model: (**a**) k-ε; (**b**) SST; (**c**) RNG k-ε; (**d**) RSM.

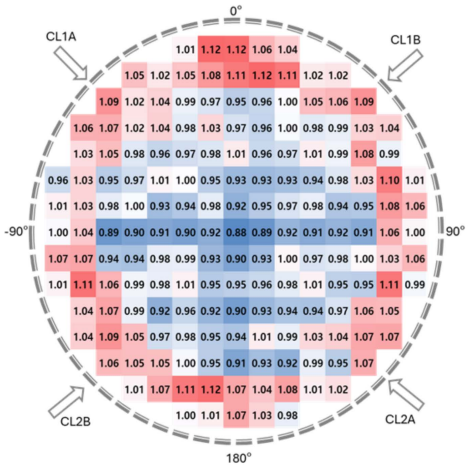

Figure 9. Core inlet flow distribution from the 1/5 scaled-down model experiment [2].

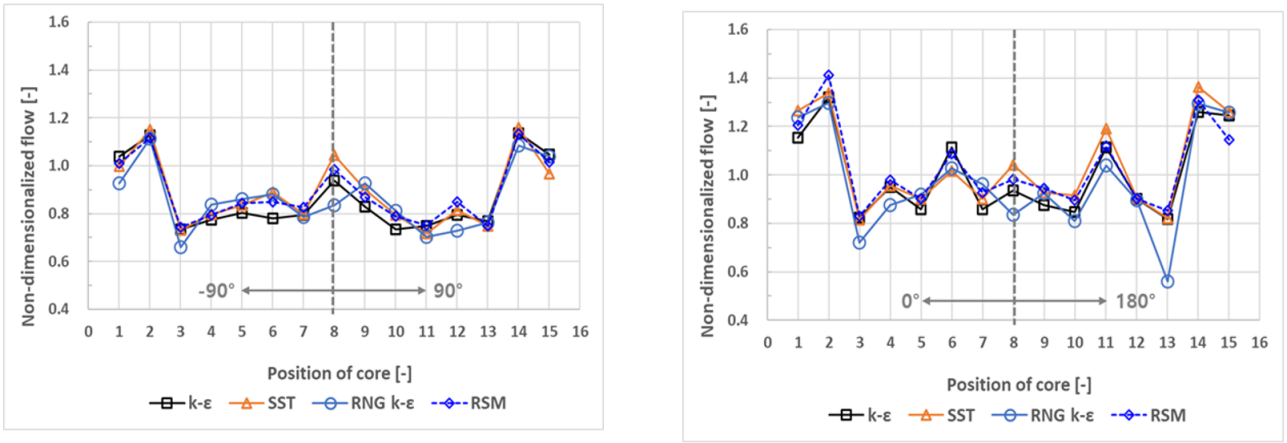

(**a**) (**b**)

Figure 10. Core inlet flow distribution along the eighth row and column for different turbulence models (FLUENT) in the 1/5 scale-down model. (**a**) Eighth row; (**b**) eighth column.

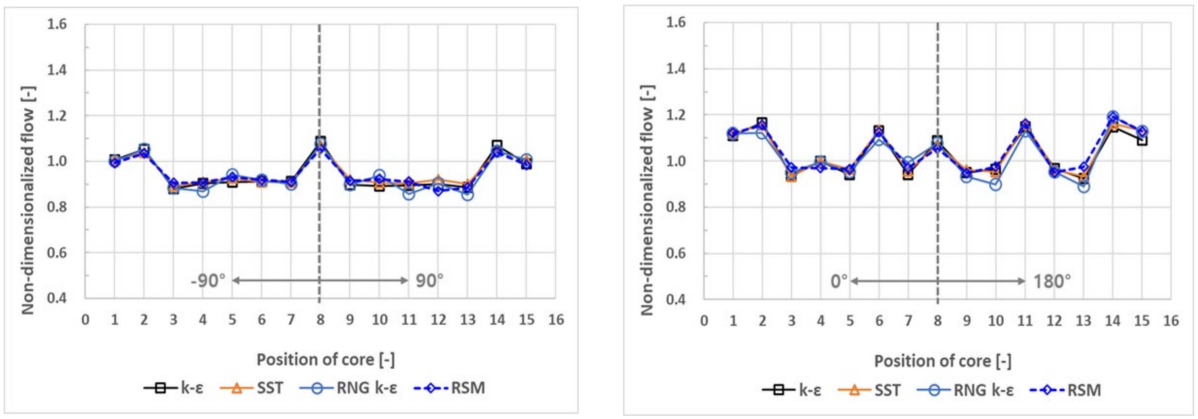

(**a**) (**b**)

Figure 11. Core inlet flow distribution along the eighth row and column for different turbulence models (CFX) in the 1/5 scale-down model. (**a**) Eighth row; (**b**) eighth column.

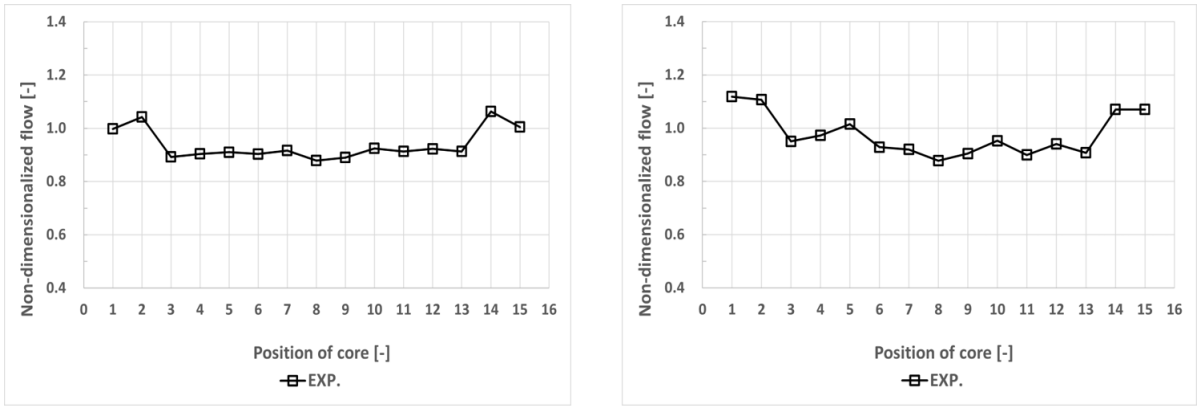

(**a**) (**b**)

Figure 12. Core inlet flow distribution along the eighth row and column from the 1/5 scaled-down model experiment: (**a**) eighth row; (**b**) eighth column [2].

Table 5 summarizes the statistical characteristics of the flow distribution according to the different turbulence models and software (Fluent/CFX) used, including comparisons with experimental results [2]. The minimum and maximum flow rates show slight differences depending on the turbulence model but generally align with the experimental ranges. The COV was 13.408–15.802% for Fluent and 7.760–8.214% for CFX, compared to the experimental COV of 5.694%, indicating slightly higher variability in the analysis results due to the turbulence models used and numerical constraints. Similarity evaluation metrics—the relative error (RD), root mean square error (RMSE), mean absolute error (MAE), and correlation coefficient (r)—were used, with both Fluent and CFX showing relatively high correlations with the experimental results. Notably, Fluent's SST and RNG k-ε models exhibited the highest similarity to the experimental data.

Overall, the choice of turbulence model and software affects the precision of the core inlet flow distribution analysis, but the main flow trends are consistently reproduced across all turbulence models. Both Fluent and CFX showed high consistency with the experimental results, with the SST and RNG k-ε models demonstrating the highest similarity to the experimental data.

Table 5. Comparison of core inlet flow distributions between turbulence models and CFD software (FLUENT and CFX) in the 1/5 scale-down model with 1/5 scaled-down experimental data.

		Fluent				CFX				Exp. [2]
		k-ε	SST	RNG k-ε	RSM	k-ε	SST	RNG k-ε	RSM	
Flow	Min. Flow Rate (-)	0.685	0.632	0.561	0.683	0.838	0.846	0.837	0.834	0.878
	Max. Flow Rate (-)	1.389	1.364	1.299	1.411	1.166	1.162	1.191	1.192	1.121
	Coefficient Of Variation (COV) (%)	15.802	14.145	13.908	13.408	8.214	7.773	7.832	7.760	5.694
Similarity	RD (-)	0.105	0.093	0.085	0.085	0.047	0.045	0.046	0.046	-
	RMSE (-)	0.122	0.110	0.107	0.103	0.064	0.062	0.062	0.063	-
	MAE (-)	0.104	0.092	0.085	0.084	0.046	0.045	0.045	0.045	-
	r (-)	0.737	0.686	0.704	0.695	0.631	0.609	0.624	0.597	-

4.2. Full-Scale Model

CFD analyses of the full-scale APR1000 reactor model's coolant flow characteristics were performed using Fluent and CFX, applying various turbulence models (standard k-ε, SST, RNG k-ε, RSM). A coarse grid was used considering computational efficiency. This study focused on evaluating the core inlet flow distribution and the uniformity of flow within the lower plenum, with key results from CFX being presented in Figures 13–16 and Table 6. Figure 13 illustrates the overall coolant flow path within the reactor, showing coolant entering through the cold legs, passing through the lower plenum, flowing through the fuel assemblies, and being discharged through the hot legs. Within the lower plenum, the coolant exhibited a tendency to be evenly distributed through structures such as the flow skirt and bottom plate, demonstrating the effective operation of reactor structures designed to induce uniform coolant distribution.

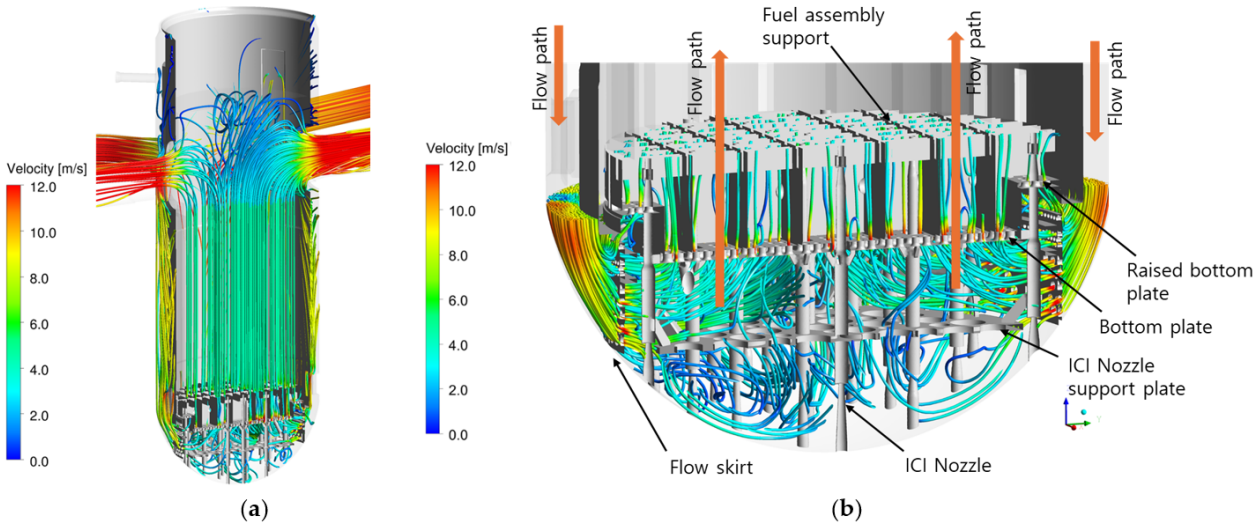

Figure 13. Coolant flow in the reactor: overall flow and lower plenum distribution: (**a**) overall coolant flow; (**b**) coolant flow in lower plenum.

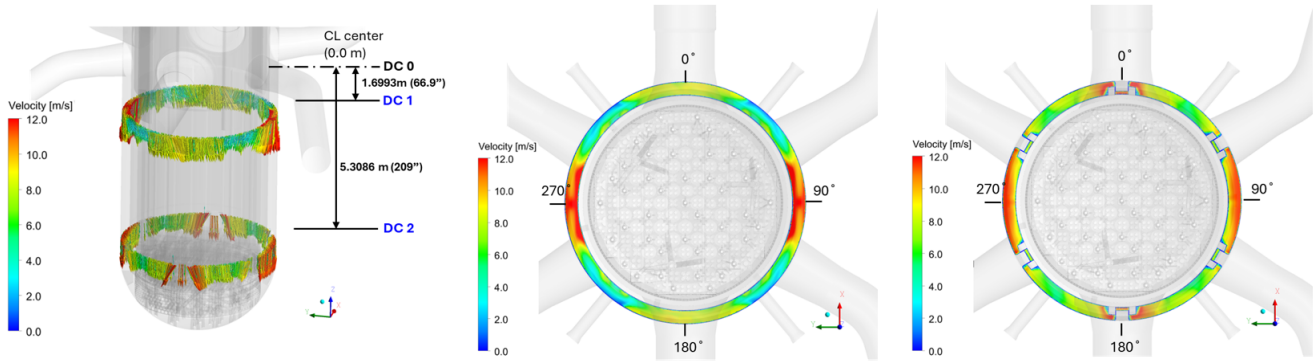

(**a**) (**b**) (**c**)

Figure 14. Velocity vectors and distribution at downcomer locations (DC 1 and DC 2): (**a**) velocity vectors (DC 1/DC 2); (**b**) velocity distribution (DC 1); (**c**) velocity distribution (DC 2).

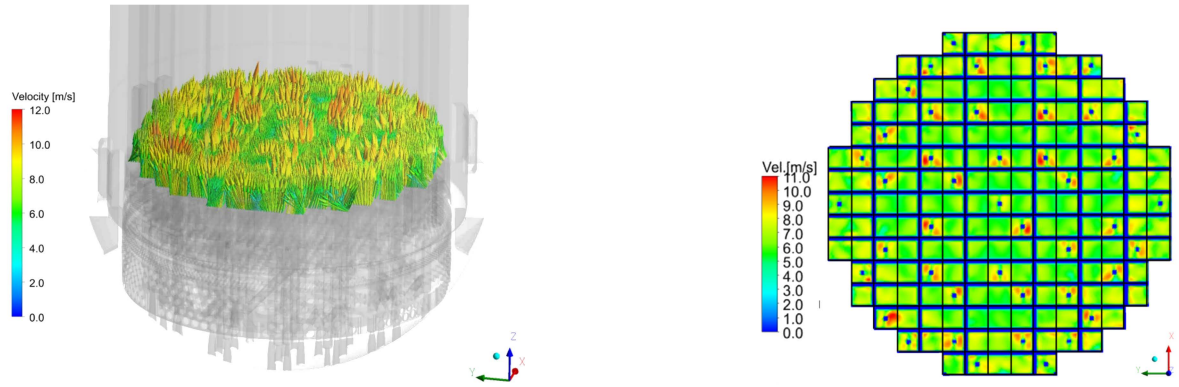

(**a**) (**b**)

Figure 15. Velocity vectors and distribution at core inlet: (**a**) velocity vectors; (**b**) velocity distribution.

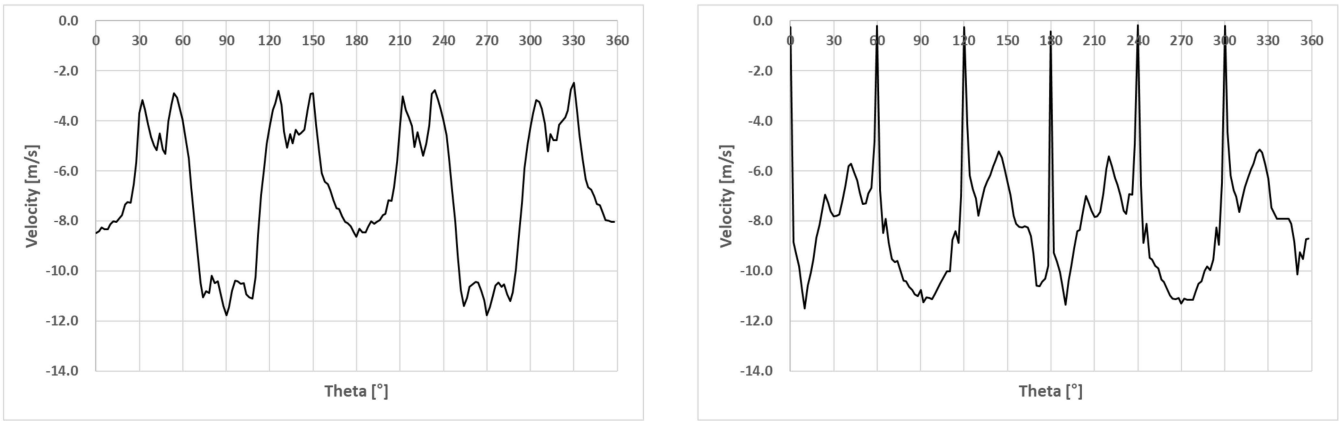

(**a**) (**b**)

Figure 16. Downward velocity at DC 1 and DC 2 locations: (**a**) DC 1; (**b**) DC 2.

Figure 14 shows velocity vectors and velocity distributions at specific heights within the downcomer (DC 1 and DC 2). Both DC 1 (upper region) and DC 2 (lower region) displayed flow adjustments to achieve uniform coolant distribution. Notably, some regions exhibited higher velocities, attributed to structural design and flow path influences. The flow distribution at the core inlet (Figure 15) maintained an overall uniform characteristic, though some local velocity changes indicated the influence of detailed structural designs.

Table 6. Effects of turbulence models on velocity and variation coefficients at DC1, DC2, and core inlet.

Model	Location	Velocity				Coefficient Of Variation (COV)
		Avg.	Max.	Min.	STD	
		(m/s)	(m/s)	(m/s)	(m/s)	(%)
k-ε	DC 1	6.848	11.762	2.472	2.715	39.7
	DC 2	8.103	11.500	0.173	2.327	28.7
	Core Inlet	1.000	1.150	0.830	0.080	8.4
SST	DC 1	6.535	11.815	1.497	2.140	32.8
	DC 2	8.107	10.522	0.152	1.828	22.5
	Core Inlet	1.000	1.170	0.840	0.080	8.0
RNG k-ε	DC 1	6.488	11.942	1.362	2.427	37.4
	DC 2	8.093	11.066	0.164	1.922	23.7
	Core Inlet	1.000	1.190	0.830	0.080	8.3
RSM	DC 1	6.507	11.962	2.138	2.283	35.1
	DC 2	7.943	9.848	0.082	1.728	21.8
	Core Inlet	1.000	1.200	0.830	0.080	7.8

Figure 16 shows the downward velocity distribution along the central line at the DC 1 and DC 2 positions based on the angle Θ, showing tendencies of coolant flow variation at specific angles. At DC 1, the velocity ranged from −2.5 m/s to −12 m/s, while at DC 2, the velocity variation significantly decreased, resulting in more uniform flow. The velocity changes at specific angles were interpreted as occurring during the flow uniformization process.

Table 6 quantitatively compares the velocity characteristics at DC 1, DC 2, and the core inlet for each turbulence model. The average velocity (avg.) was the highest for the standard k-ε model at DC 1 and for the SST model at DC 2. Based on the standard deviation (STD) and COV, the SST model exhibited lower variability compared to the other models, providing relatively uniform flow distribution. At the core inlet, all turbulence models showed a COV below 8%, confirming that the flow distribution remained generally uniform.

Overall, the structural design within the lower plenum effectively induced a uniform distribution of coolant flow, and the flow distribution at the core inlet was stably maintained. The SST and RNG k-ε models demonstrated a relatively high accuracy and flow uniformity.

To evaluate the sensitivity of the flow distribution to the turbulence models in the full-scale APR1000 reactor model, key results are presented in Figures 17–20 and Table 7, comparing Fluent and CFX analyses. The Fluent analysis results (Figure 17) show distinct flow distribution characteristics for each turbulence model. The SST and RNG k-ε models accurately reproduced high flow rates at the core periphery and low flow rates at the center, effectively reflecting the uniformity and local features of the flow distribution. In contrast, the standard k-ε model and RSM exhibited similar main flow trends but showed some discrepancies in local flow variations compared to the experimental results (Figure 9). These findings indicate that the SST and RNG k-ε models in Fluent most accurately reproduce the core inlet flow characteristics. Similar trends were observed in the CFX analysis results (Figure 18), with the SST and RNG k-ε models showing the highest similarity. Specifically, the SST model minimized the flow distribution variability and maintained an overall uniform distribution, closely matching the experimental results. While the standard k-ε model and RSM produced similar trends to Fluent, they exhibited relatively larger discrepancies in local flow variations. The CFX analysis results showed higher consistency with the experimental results compared to Fluent.

Figures 19 and 20 show the dimensionless flow distribution at the eighth row and eighth column, respectively. Both Fluent and CFX showed that the SST and RNG k-ε models had high similarity to the experimental data, with the SST model most accurately reproducing both the local flow changes and the overall distribution. CFX demonstrated lower variability than Fluent, resulting in a higher consistency with the experimental data.

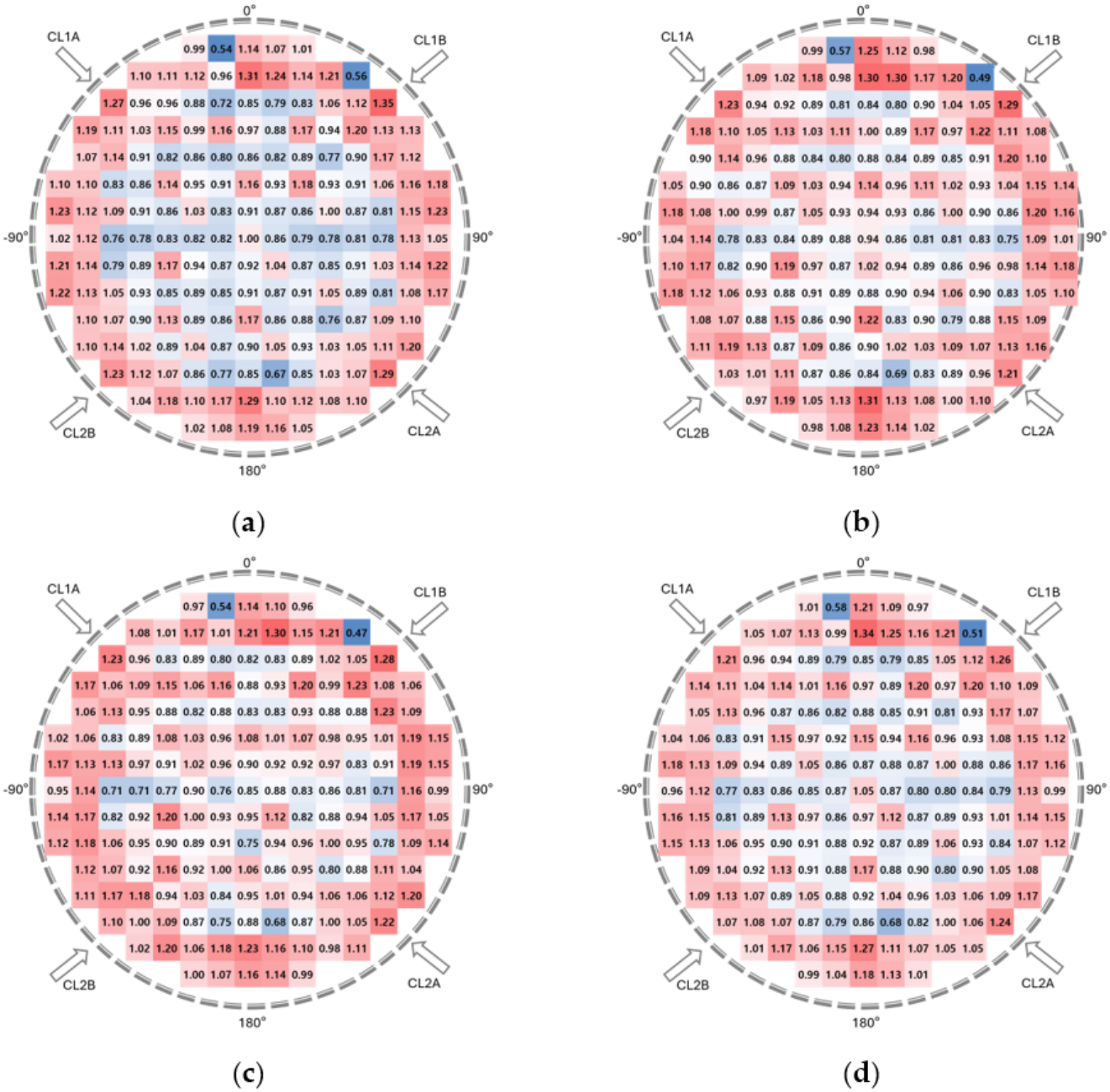

Figure 17. Core inlet flow distribution according to turbulence models (Fluent): (**a**) k-ε; (**b**) SST; (**c**) RNG k-ε; (**d**) RSM.

The quantitative analysis results in Table 7 compare the flow distribution statistics across the turbulence models and Fluent/CFX software. For the minimum and maximum flow rates, Fluent reported ranges from 0.470 (0.537) to 1.304 (1.348), while CFX reported ranges from 0.827 (0.845) to 1.154 (1.195). Compared to the scaled-down experimental data (minimum 0.878, maximum 1.121), CFX showed higher accuracy. In the COV analysis, Fluent's SST model had the lowest COV at 14.164%, and CFX's SST model had the lowest at 7.993%, closely matching the experimental COV of 5.694%. This indicates that CFX

better reflects the uniformity of flow distribution compared to Fluent. Similarity metrics analysis showed that the SST and RNG k-ε models had the highest correlations with the experimental data. In Fluent, the SST model had a relative error (RD) of 0.089, an RMSE of 0.116, an MAE of 0.089, and a correlation coefficient (r) of 0.607, while the RNG k-ε model exhibited similar trends. In CFX, the SST model achieved an RD of 0.047, an RMSE of 0.064, an MAE of 0.046, and an r of 0.623, demonstrating the best performance, with the RNG k-ε model also showing high consistency with the experimental data.

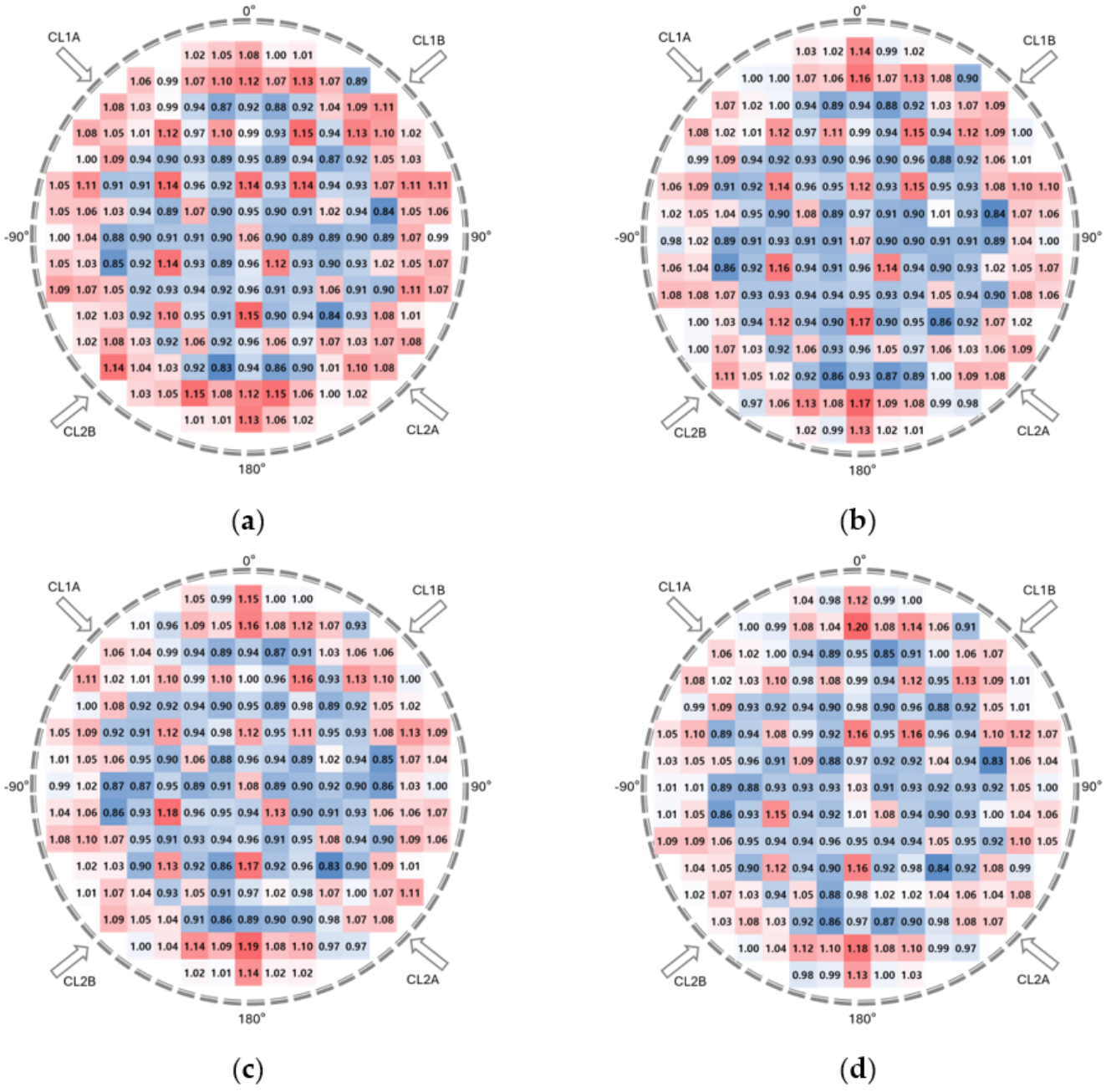

Figure 18. Core inlet flow distribution according to turbulence models (CFX): (**a**) k-ε; (**b**) SST; (**c**) RNG k-ε; (**d**) RSM.

The scaled-down model experiments were conducted according to similarity laws, ensuring meaningful comparisons between the experimental data and full-scale model analysis results. Both the Fluent and CFX analyses using the SST and RNG k-ε models showed high similarity to the scaled-down experimental results, with CFX's SST model

providing the best agreement in terms of the minimum and maximum flow rates, COV, and similarity metrics. Overall, the SST and RNG k-ε models were deemed suitable turbulence models for accurately analyzing the core inlet flow distribution of the APR1000 reactor in both Fluent and CFX. CFX demonstrated higher accuracy compared to Fluent, and the SST model proved to be the most reliable analytical tool. These findings provide essential foundational data for optimizing reactor design and safety assessments and offer a basis for validating CFD analysis methodologies through comparisons with scaled-down experimental results.

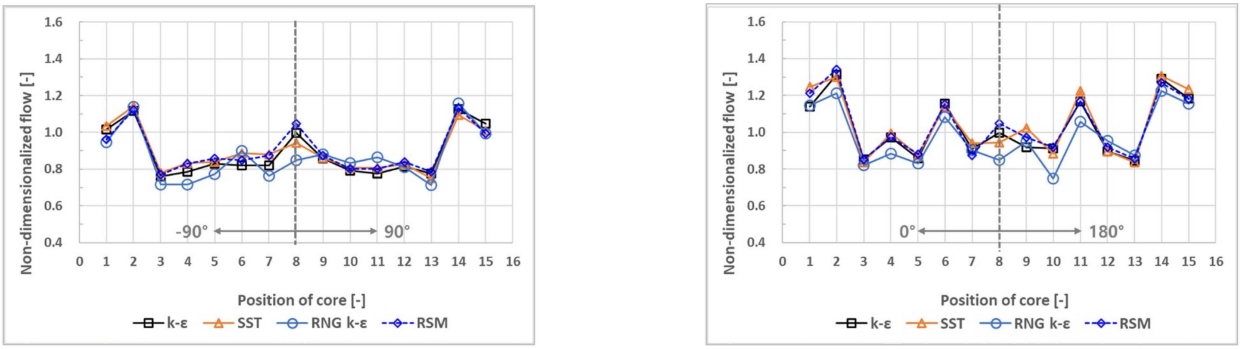

(**a**) (**b**)

Figure 19. Core inlet flow distribution along the eighth row and column for different turbulence models (Fluent): (**a**) eighth row; (**b**) eighth column.

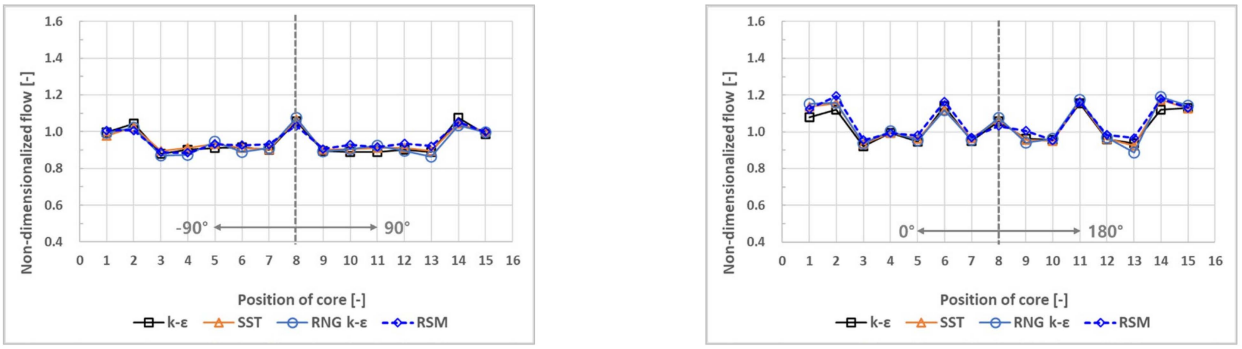

(**a**) (**b**)

Figure 20. Core inlet flow distribution along the eighth row and column for different turbulence models (CFX): (**a**) eighth row; (**b**) eighth column.

Table 7. Comparison of core inlet flow distribution between turbulence models and CFD software (FLUENT and CFX) with the 1/5 scaled-down model experimental data.

		Fluent				CFX				Exp. [2]
		k-ε	SST	RNG k-ε	RSM	k-ε	SST	RNG k-ε	RSM	
Flow	Min. Flow Rate (-)	0.537	0.489	0.470	0.509	0.827	0.845	0.828	0.831	0.878
	Max. Flow Rate (-)	1.348	1.308	1.304	1.340	1.154	1.174	1.189	1.195	1.121
	Coefficient Of Variation (COV) (%)	15.307	14.164	14.332	13.726	8.370	7.993	8.250	7.787	5.694

Table 7. *Cont.*

		Fluent				CFX				Exp. [2]
		k-ε	**SST**	**RNG k-ε**	**RSM**	**k-ε**	**SST**	**RNG k-ε**	**RSM**	
Similarity	RD (-)	0.100	0.089	0.087	0.085	0.049	0.047	0.049	0.047	-
	RMSE (-)	0.126	0.116	0.118	0.112	0.066	0.064	0.066	0.065	-
	MAE (-)	0.100	0.089	0.087	0.085	0.048	0.046	0.049	0.046	-
	r (-)	0.619	0.607	0.610	0.604	0.623	0.601	0.602	0.577	-

5. Conclusions

This study conducted CFD analyses of the core inlet flow distribution in the APR1000 reactor and validated the reliability of the CFD analysis methodology by applying various turbulence models (standard k-ε, SST, RNG k-ε, RSM). The analyses were performed using the Fluent and CFX software, and the validity of the analytical methods was verified by comparing the results with experimental data from the scaled-down model before extending the methodology to the full-scale model to analyze core inlet flow characteristics.

Comparisons with the scaled-down model experimental results revealed that the SST and RNG k-ε models exhibited the highest consistency with the experimental data. The SST model minimized the flow distribution variability and accurately reproduced local flow changes in both Fluent and CFX. Notably, CFX's SST model showed the best agreement with the experimental data in terms of the minimum and maximum flow rates, COV, and similarity metrics (RD, RMSE, MAE, r). These results demonstrate that the SST model is the most reliable turbulence model for analyzing the core inlet flow distribution of the APR1000 reactor. The RNG k-ε model also performed similarly to the SST model, making both models suitable for extending the scaled-down experimental results to the full-scale model. In contrast, the standard k-ε model and RSM, while accurately reproducing main flow trends, showed a somewhat lower performance in accurately depicting local flow distributions compared to the SST and RNG k-ε models.

In the full-scale model analysis, the SST and RNG k-ε models accurately predicted the core inlet flow distribution, maintaining uniformity between the core periphery and the center. Within the lower plenum, the coolant exhibited a tendency to be evenly distributed through structures such as the flow skirt, bottom plate, and raised bottom plate, confirming that these structural designs effectively contribute to the uniform distribution of coolant. Specifically, the analysis of the velocity distribution at the downcomer locations showed that the process of flow uniformization within the lower plenum formed a stable flow distribution at the core inlet. This indicates that the APR1000 reactor's coolant design effectively ensures uniform cooling for each fuel assembly.

The quantitative analysis results revealed that CFX showed higher correlation with the experimental data compared to Fluent. When using the SST model in CFX, the COV was 7.993%, closely matching the experimental COV of 5.694%. Additionally, the SST model in CFX achieved the lowest relative error (RD) of 0.047 and the lowest root mean square error (RMSE) of 0.064, demonstrating high consistency with the experimental data. These results indicate that CFX provides higher precision in simulating the complex thermal-fluid characteristics of the reactor compared to Fluent.

The comparison with scaled-down model experiments played a crucial role in enhancing the reliability of the CFD analysis methodology. The scaled-down experiments, conducted according to appropriate similarity laws, provided meaningful data that were comparable to full-scale model analysis results. Both the SST and RNG k-ε models showed high similarity to the scaled-down experimental results in both Fluent and CFX, demon-

strating that the same analytical methods could be reliably applied to the full-scale model. Specifically, the scaled-down experimental data served as a useful benchmark for evaluating and validating the analysis results of the full-scale model, effectively complementing the experimental limitations with CFD analysis.

In conclusion, the CFD analysis methodology established in this study was evaluated as a reliable tool for analyzing the core inlet flow distribution of the APR1000 reactor. The SST and RNG k-ε models demonstrated high similarity with the experimental data in both Fluent and CFX, with CFX's SST model providing the most accurate analysis results. These findings offer essential foundational data for optimizing reactor design and safety assessments and confirm the high reliability of analysis of the full-scale model through comparisons with scaled-down experimental results. The CFD analysis methodology developed in this study can be extended to other reactor designs and analyses, serving as a critical guideline for the design and analysis of complex thermal-fluid systems.

Author Contributions: Conceptualization, C.C. and D.K.C.; methodology, S.M.S.; software, S.M.S.; validation, S.M.S., D.K.C. and C.C.; formal analysis, D.K.C.; investigation, S.M.S.; resources, C.C.; data curation, W.M.P.; writing—original draft preparation, S.M.S.; writing—review and editing, W.M.P. and C.C.; visualization, S.M.S.; supervision, C.C.; project administration, C.C. All authors have read and agreed to the published version of the manuscript.

Funding: This work was supported by the Korea Institute of Energy Technology Evaluation and Planning (KETEP) and the Ministry of Trade, Industry & Energy (MOTIE) of the Republic of Korea (No. 20217810100010).

Data Availability Statement: The data presented in this study are available on request from the corresponding author. The data are not publicly available due to design information security.

Conflicts of Interest: All authors are from Company "ELSOLTEC". The authors declare no conflicts of interest.

References

1. Kim, K.; Kim, K.-M.; Choi, H.-S.; Seol, H.; Lim, B.-J.; Kim, W.-S.; Euh, D.-J. Experimental Study of the Lower Support Structure Effect on the Core Flow Distribution. *KSFM J. Fluid Mach.* **2024**, *27*, 24–30. [CrossRef]
2. Kim, K.; Kim, W.-S.; Choi, H.-S.; Seol, H.; Lim, B.-J.; Euh, D.-J. An Experimental Evaluation of the APR1000 Core Flow Distribution Using a 1/5 Scale Model. *Energies* **2024**, *17*, 2714. [CrossRef]
3. Bae, Y.; Kim, Y.I.; Park, C.T. CFD Analysis of Flow Distribution at the Core Inlet of SMART. *Nucl. Eng. Des.* **2013**, *258*, 19–25. [CrossRef]
4. Xu, S.; Yue, J.; Zhang, J.; Li, D.; Tian, R.; Tan, S. Numerical Analysis on Flow Distribution of Nuclear Reactor Core Inlet under Ocean Conditions. *Nucl. Eng. Des.* **2023**, *414*, 112576. [CrossRef]
5. Zeng, J.; Mao, Y.; Li, B.; Zhu, J.; Hu, Y.; Chen, J. Analysis of Coolant Flow Distribution Characteristics at Core Inlet of Small Pressurized Water Reactor under Rolling Condition. *Front. Energy Res.* **2024**, *11*, 1324187. [CrossRef]
6. Kim, K.; Euh, D.-J.; Chu, I.-C.; Youn, Y.-J.; Choi, H.-S.; Kwon, T.-S. Experimental Study of the APR+ Reactor Core Flow and Pressure Distributions under 4-Pump Running Conditions. *Nucl. Eng. Des.* **2013**, *265*, 957–966. [CrossRef]
7. Suh, J.M.; Park, N.G.; Jeon, K.L.; Hwang, S.T. Development of a Hiper PWR Fuel Assembly for OPR1000 and APR1400. In Proceedings of the 18th Pacific Basin Nuclear Conference, Busan, Republic of Korea, 18–23 March 2012; pp. 18–23.
8. Karpenko, M. Aircraft Hydraulic Drive Energy Losses and Operation Delay Associated with the Pipeline and Fitting Connections. *Aviation* **2024**, *28*, 1–8. [CrossRef]
9. Dhaubhadel, M.N. Review: CFD Applications in the Automotive Industry. *J. Fluids Eng.* **1996**, *118*, 647–653. [CrossRef]
10. Mrope, H.A.; Jande, Y.A.C.; Kivevele, T.T. A Review on Computational Fluid Dynamics Applications in the Design and Optimization of Crossflow Hydro Turbines. *J. Renew. Energy* **2021**, *2021*, 5570848. [CrossRef]
11. Ettehadi, A.; Altun, G. A Review of Application of Computational Fluid Dynamics in Prediction of Oil and Gas Wells Problems. In Proceedings of the 19th International Petroleum and Natural Gas Congress and Exhibition of Turkey, Ankara, Turkey, 15–17 May 2013. [CrossRef]
12. Kang, K.; Wang, X.; Wang, J.; Shi, W.; Sun, Y.; Chen, M. A Critical Review of a Computational Fluid Dynamics (CFD)-Based Explosion Numerical Analysis of Offshore Facilities. *Arch. Comput. Methods Eng.* **2022**, *29*, 4851–4870. [CrossRef]

13. Wijesooriya, K.; Mohotti, D.; Lee, C.K.; Mendis, P. A Technical Review of Computational Fluid Dynamics (CFD) Applications on Wind Design of Tall Buildings and Structures: Past, Present and Future. *J. Build. Eng.* **2023**, *74*, 106828. [CrossRef]
14. Liu, J.; Zhu, S.; Kim, M.K.; Srebric, J. A Review of CFD Analysis Methods for Personalized Ventilation (PV) in Indoor Built Environments. *Sustainability* **2019**, *11*, 4166. [CrossRef]
15. Norton, T.; Sun, D.W. Computational Fluid Dynamics (CFD)—An Effective and Efficient Design and Analysis Tool for the Food Industry: A Review. *Trends Food Sci. Technol.* **2006**, *17*, 600–620. [CrossRef]
16. Raman, R.K.; Dewang, Y.; Raghuwanshi, J. A Review on Applications of Computational Fluid Dynamics. *Int. J. LNCT* **2018**, *2*, 137–143.
17. Mohamadi, F.; Fazeli, A. A Review on Applications of CFD Modeling in COVID-19 Pandemic. *Arch. Comput. Methods Eng.* **2022**, *29*, 3567–3586. [CrossRef]
18. Keir, G.; Jegatheesan, V. A Review of Computational Fluid Dynamics Applications in Pressure-Driven Membrane Filtration. *Rev. Environ. Sci. Biotechnol.* **2014**, *13*, 183–201. [CrossRef]
19. Zigh, G.; Gonzalez, S. *Validation of Computational Fluid Dynamics Methods Using Prototypic Light Water Reactor Spent Fuel Assembly Thermal-Hydraulic Data (NUREG-2208)*; Office of Nuclear Regulatory Research, U.S, Nuclear Regulatory Commission: Rockville, MD, USA, 2017.
20. Wang, M.; Wang, Y.; Tian, W.; Qiu, S.; Su, G.H. Recent Progress of CFD Applications in PWR Thermal Hydraulics Study and Future Directions. *Ann. Nucl. Energy* **2021**, *150*, 107836. [CrossRef]
21. Tian, W.; Wang, M.; Petrov, V.; Erkan, N.; Liao, Y. Editorial: CFD Applications in Nuclear Engineering. *Front. Energy Res.* **2021**, *9*, 630305. [CrossRef]
22. IAEA Nuclear Energy Series. *Summary Review on the Application of Computational Fluid Dynamics in Nuclear Power Plant Design, International Atomic Energy Agency No. NR-T-1.20*; IAEA Nuclear Energy Series 2022; International Atomic Energy Agency: Vienna, Austria, 2022.
23. Wang, M.; Ju, H.; Wu, J.; Qiu, H.; Liu, K.; Tian, W.; Su, G.H. A Review of CFD Studies on Thermal Hydraulic Analysis of Coolant Flow through Fuel Rod Bundles in Nuclear Reactor. *Prog. Nucl. Energy* **2024**, *171*, 105175. [CrossRef]
24. Lee, G.H.; Bang, Y.S.; Woo, S.W.; Kim, D.H.; Kang, M.G. Numerical Analysis of Internal Flow Distribution in Scale-Down APR+. Trans. Korean Soc. *Mech. Eng. B* **2013**, *37*, 855–862.
25. Kutuk, B.; Guzelbey, I.H. Computational Fluid Dynamics Analyses of a VVER-1200 Nuclear Reactor Vessel for Symmetric Inlet, Asymmetric Inlet, and LOCA Conditions. *Int. J. Press. Vessel. Pip.* **2020**, *187*, 104165. [CrossRef]
26. Wang, L.; Deng, J.; Wang, M.; Zhang, D.; Qiu, S.; Su, G.H.; Tian, W. Numerical Simulation of Temperature Heterogeneity Inside the AP1000 Upper Plenum and Hot Leg. *Nucl. Eng. Des.* **2020**, *362*, 110525. [CrossRef]
27. Puragliesi, R.; Zhou, L.; Zerkak, O.; Pautz, A. Steady-State CFD Simulations of an EPR™ Reactor Pressure Vessel: A Validation Study Based on the JULIETTE Experiments. *Nucl. Eng. Des.* **2016**, *300*, 41–56. [CrossRef]
28. Lee, G.H.; Bang, Y.S.; Cheong, A.J. Numerical Analysis of Flow Distribution in the Scale-Down APR+ Using Two-Equation Turbulence Models. *Korean J. Air-Cond. Refrig. Eng.* **2015**, *27*, 220–227.